NJC

PAPER

Check for updates

A coumarin-based reversible fluorescent probe for Cu²⁺ and S²⁻ and its applicability *in vivo* and for organism imaging†

Wen Lu, [ID] *[a] Jiuzhou Shi,[a] Jichao Chen,[b] Lu Sun,[a] Lingcen Shao,[a] Hongyu Ren,[a] Mengmeng Huang,[a] Yanqin Wang,[a] Shilong Yang[c] and Xu Li [ID] *[a]

This study describes the synthesis of a coumarin-based reversible fluorescent probe **BuCAC** for the detection of Cu²⁺ and S²⁻ in CH₃CN : PBS (v/v = 8 : 2, pH = 7.4) solution. The resulting **BuCAC** exhibited high sensitivity (detection limit = 3.03×10^{-7} M) and selectivity towards Cu²⁺ through a 2 : 1 binding mode. In the presence of S²⁻, the **BuCAC–Cu²⁺** recovered to BuCAC and CuS, which in turn perform the function of a sensitive probe with a lower detection limit of about 1.7×10^{-7} M. This "on–off–on" process can easily occur in 1 min with a repetition of at least 5 times. The sensing mechanism was confirmed by Job's plot analysis, MS, and density theory calculation. Besides, fluorescence imaging in zebrafish, HeLa cells, and soybean root tissue revealed that the probe BuCAC could serve as a valuable tool for monitoring and tracking intracellular Cu²⁺ and S²⁻ while benefiting from its excellent fluorescence performance and lower cytotoxicity.

1. Introduction

Copper is one of the earliest metals discovered by humans and has been widely used in mechanical, electrical, construction, and decoration applications.[1–3] Due to their unique redox activity, copper ions serve as an important co-catalytic factor that significantly participates in the synthesis of multiple metal enzymes, such as cytochrome oxidase, tyrosinase, and copper/zinc superoxide dismutase.[4,5] Excessive intake of copper ions can cause severe damage to the internal organs of the human body, especially the liver and bile, as well as adversely affect the metabolic pathways of the body.[6–8] A range of diseases including necrotum hepatitis and hemolytic anemia are associated with copper poisoning.[9] Additionally, copper poisoning also causes significant damage to the nervous system,[10] digestive system,[11] cardiovascular system,[12,13] and various other systems.[14–16] Therefore, the rapid and accurate detection of this toxic substance is of great importance to maintain human health and life. Until now, a variety of structures have been reported for use as fluorescent probes for the detection of Cu²⁺, such as acridine,[17] quinoline,[18] rhodamine,[19–22] salicylaldehyde,[23] BODIPY,[24] coumarin,[25–27] MOF[28,29] and so on. Besides, S²⁻ is another hazardous and toxic

pollutant with significant adverse effects on daily life. Increased levels of S²⁻ are more likely to cause a variety of physiological problems which include respiratory paralysis, unconsciousness, and irritation in the mucous membrane.[30] Furthermore, it is also interconnected to various diseases, diabetes, and Down syndrome.[31–34] Therefore, it is highly required to explore a rapid and convenient method to monitor Cu²⁺ and S²⁻ in the natural environment.

Previously, atomic absorption spectroscopy, electrochemical analysis, colorimetry, and gas chromatography have been reported to detect Cu²⁺ and S²⁻.[35–40] Fluorescence sensing technology has attracted greater attention over traditional analysis methods because of its simple and convenient operation. So far, various Cu²⁺ and S²⁻ fluorescent probes have been actively explored.[41–45]

Owing to the rapid combination of a copper ion (Cu²⁺) and sulfide ion (S²⁻) to form a stable compound, copper sulfide (CuS, $K_{sp} = 6.3 \times 10^{-36}$),[46] here we describe the design and development of a coumarin-based novel fluorescent probe, **BuCAC**. The sensing mechanism was studied using a Job's curve, mass spectrometry experiments, and theoretical calculations. It was effectively utilized to detect Cu²⁺ and S²⁻ in HeLa cells, zebrafish, and soybean root tissue (Scheme 1).

2. Experimental section

2.1. Materials and instruments

All the reagents and chemicals used in experiments were purchased from Aladdin and were used without further

[a] *College of Science, Nanjing Forestry University, Nanjing, Jiangsu, 210037, China. E-mail: luwen@njfu.edu.cn, xuliqby@njfu.edu.cn*

[b] *College of Chemical Engineering, Nanjing Forestry University, Nanjing, Jiangsu, 210037, China*

[c] *Advanced Analysis and Testing Center, Nanjing Forestry University, Nanjing, Jiangsu, 210037, China*

† Electronic supplementary information (ESI) available. See DOI: 10.1039/d1nj01951a
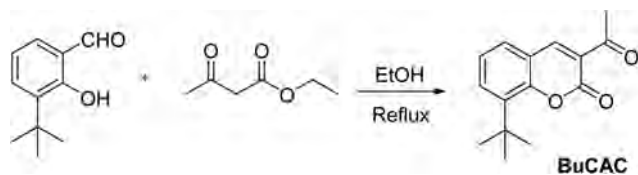
Scheme 1   The synthetic route of **BuCAC**.

purification. Deionized water was used as the aqueous medium in this research.

Fluorescence spectra and UV-vis spectra were observed using an LS 55 Fluorescence Spectrometer with a 1 cm square quartz cell (PerkinElmer) and a LAMBDA950 spectrometer (PerkinElmer Precisely), respectively. FTIR spectra of the samples were recorded with a Bruker Vertex 80v spectrophotometer at room temperature after diluting the samples with KBr. NMR spectra were recorded on a Bruker AVANCE III HD spectrometer operating at 600 MHz. Mass spectrometry was performed on an LTQ-Orbitrap (Thermo Fisher Scientific). The final bioimaging application was measured using a Zeiss LSM710 Airy scan confocal laser scanning microscope.

2.2.   Synthesis of 3-acetyl-8-*tert*-butyl coumarin (BuCAC)

40 ml of absolute ethanol, 0.6 ml of 3-*tert*-butylsalicylic aldehyde, 0.3 ml of ethyl acetoacetate, 5 drops of glacial acetic acid, and 5 drops of piperidine were added to a 100 ml round bottom flask in sequence, and the mixed solution was heated to reflux for 5 hours. After cooling overnight at room temperature, a light-yellow solid was obtained after suction filtration. The crude product was recrystallized from absolute ethanol to obtain a white solid. 0.36 g, yield 73.2%, m.p. 158 °C. IR(KBr) ν_{max} (cm^{-1}): 3072(Ar-H), 2966, 2875(–C(CH$_3$)$_3$), 1737(–C=O) cm^{-1}. ^{1}H NMR (DMSO-d_6, 600M): δ 8.654 (s, 1H, C=CH–), 7.831–7.819 (d, J = 7.2Hz, 1H, Ar-H), 7.693–7.681 (d, J = 7.2Hz, 1H, Ar-H), 7.357 (m, 1H, Ar-H), 2.607 (s, 3H, –CH$_3$), 1.464 (s, 9H, –C(CH$_3$)$_3$); ^{13}CNMR (CDCl$_3$, 150 MHz): δ 195.590, 158.898, 154.142, 148.416, 138.063, 132.025, 128.625, 124.574, 123.504, 118.756, 35.011, 30.622, 29.756. MS (ESI) m/z calculated for $[M + H]^+$ 245.12; found 245.12. Characterization of **BuCAC** is shown in Fig. S1–S4 (ESI†).

2.3.   Spectral measurements

The stock solutions (1 mM) of various cations (Ca^{2+}, Al^{3+}, Cd^{2+}, Cr^{3+}, Co^{2+}, Cu^{2+}, Fe^{3+}, Fe^{2+}, K$^+$, Mn^{2+}, Mg^{2+}, Na$^+$, Zn^{2+}, and Pb^{2+}) and anions (F$^-$, Cl$^-$, Br$^-$, I$^-$, S^{2-}, NO$_3^-$, SO$_3^{2-}$, HSO$_4^-$, H$_2$PO$_4^-$, ClO$_4^-$ and CH$_3$COO$^-$) were prepared in deionized water and the probe **BuCAC** was the same concentration as the salt solution in acetonitrile. The excitation wavelength of 305 nm was selected for the fluorescence spectrum test (λ_{ex} = 305 nm, slit width: 5, 5 nm). In the experimental titration, the probe solution (3 ml) present in the quartz optical cell was subjected to titration with Cu^{2+}/S^{2-} prepared in advance. To assure the reproducibility of the results, all experiments were performed 2–3 times.

2.4.   Bioimaging in cells

HeLa cells were incubated at 37 °C in 5% CO$_2$. The medium (10% FBS and 5% penicillin–streptomycin mixed solution) was removed after 24 h of the experiment and the cells were washed thrice with PBS (pH = 7.2). The cells were then divided into three different groups: the first group was treated with **BuCAC** (10 μM) followed by incubation for 1 h. The second group was treated with **BuCAC** (10 μM) and 10 μM Cu^{2+} solution and co-incubated for 60 min. The third group was treated with **BuCAC** (10 μM), Cu^{2+} (10 μM), and S^{2-} (10 μM), and incubated for 60 min. Fluorescence imaging was carried out with the help of a confocal laser scanning fluorescence microscope.

2.5.   Bioimaging in zebrafish and soybean root tissues

Two different samples of soybean root tissues and zebrafish were chosen for bioimaging. Zebrafish were incubated in a nutrient solution followed by the preparation of two sets of blanks (containing Cu^{2+} (10 μM) or not) for 0.5 h. After washing with PBS three times, both groups were treated with **BuCAC** (10 μM) for 0.5 h. Then, the bioimaging of zebrafish of both groups was performed by using confocal microscopy upon the addition of Cu^{2+} and S^{2-}. Plant cell imaging was also performed by using soybean root tissue. Soybean seeds were subjected to sterilization with alcohol and then allowed to culture at room temperature in moist medium. The experimental procedure was similar to that carried out for zebrafish.

2.6.   Quantum calculations

All calculations were performed using the Gaussian 16 software package.[47] The density functional theory with dispersion correction (DFT-D3) method, mode B3LYP, was used to optimize the geometry of the ground state structure before and after the reaction between **BuCAC** and Cu^{2+} ions (Fig. S6 and S7, ESI†),[48–51] and the excited state geometry was optimized at the B3LYP/ 6-311G(d) level. The nature of absorption and emission was studied by using natural transition orbital (NTO) analysis which was based on DFT calculations and the calculated transition density matrices.[52] The solvation effect was considered using the SMD solvation model in all the calculations used in the study;[53] the 6-311G(d) basis set for the atoms C, H, and O, and the SDD basis set for Cu were selected.

3.   Results and discussion

3.1.   Fluorescence response of BuCAC towards Cu^{2+}

The optical properties of the probe **BuCAC** and its response to copper ions were evaluated in CH$_3$CN : PBS (v/v = 8 : 2, pH = 7.4, 10 μM) solution. Fig. 1a shows the strong fluorescence emission of **BuCAC** at 419 nm. After the incorporation of Cu^{2+}, the intensity of fluorescence at 419 nm gradually decreased, which may be attributed to the reaction of Cu^{2+} with the probe to form **BuCAC**–Cu^{2+}. As a result, the changes occurred in the transition mode of excited electrons of the probe with a frequent decrease in fluorescence because of the paramagnetism of Cu^{2+}. Moreover, a linear relationship was observed between the change in the fluorescence intensity and the concentration of Cu^{2+} over a range of 0–28.6 μM, the linear equation is $y = -10.577x + 474.84$, and the linear fitting constant $R^2 = 0.984$ (Fig. 1b). The detection limit was
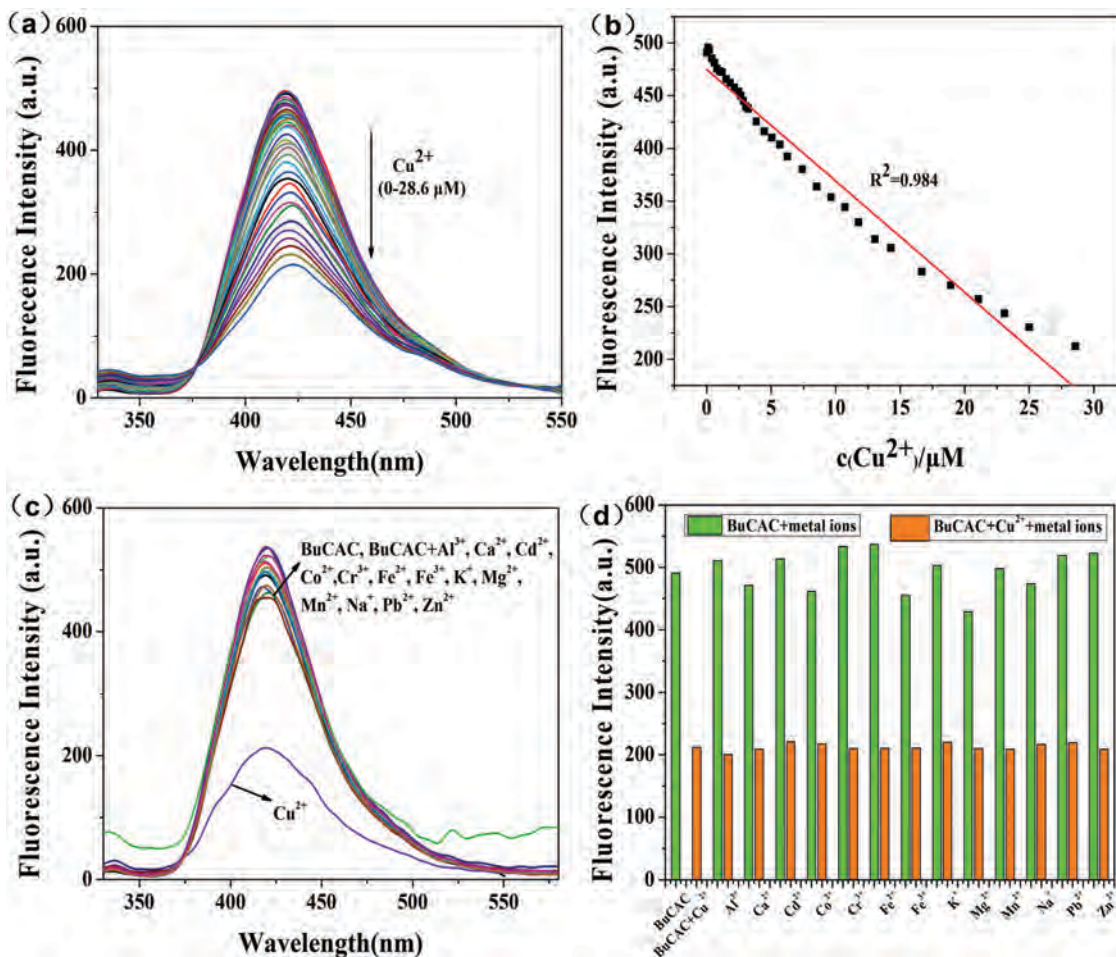
Fig. 1 (a) Fluorescence spectra of BuCAC (10 μM) to Cu^{2+} in CH_3CN : PBS (v/v = 8 : 2, pH = 7.4) solution. (λ_{ex} = 305 nm, slit width: 5, 5 nm). (b) Linear relationship between the fluorescence intensity and concentration range of Cu^{2+} (0–28.6 μM). (c) Emission spectra of **BuCAC** (10 μM) upon the addition of different metal ions (100 μM) in CH_3CN : PBS (v/v = 8 : 2, pH = 7.4) solution. (λ_{ex} = 305 nm, slit width: 5, 5 nm). (d) Fluorescence spectra of **FL** in the presence of interfering metal ions in CH_3CN : PBS (8 : 2, v/v) solution. (λ_{ex} = 305 nm, slit width: 5, 5 nm).

found to be 3.03×10^{-7} M, indicating that the probe **BuCAC** has high sensitivity to copper ions and has the potential to detect the changes in trace copper ions *in vivo*.

3.2. Selectivity of BuCAC for Cu^{2+}

Selectivity is an essential requirement for the specific detection of target species. For this purpose, competitive metal ions were also incorporated into the solution of **BuCAC**–Cu^{2+} to examine if **BuCAC** responds to other metal ions or not. The results showed that the fluorescence intensity of BuCAC only decreases upon the addition of Cu^{2+}, while all the tested cations (Ca^{2+}, Al^{3+}, Cd^{2+}, Cr^{3+}, Co^{2+}, Cu^{2+}, Fe^{3+}, Fe^{2+}, K^+, Mn^{2+}, Mg^{2+}, Na^+, Zn^{2+}, and Pb^{2+}) produced negligible changes in fluorescence (Fig. 1c). Hence, after adding other metal ions to the BuCAC–Cu^{2+} solution, the fluorescence intensity remained at about 200 (Fig. 1d), which not only justifies the selectivity of BuCAC to copper ions but also shows the good anti-interference ability of BuCAC. It can be inferred from the results that the probe under consideration can be used in complex environments.

3.3. Fluorescence response of BuCAC–Cu^{2+} systems with S^{2-}

Cu^{2+} can easily be removed from **BuCAC**–Cu^{2+} after the addition of S^{2-} because of the significantly higher binding constant of CuS than that of **BuCAC**–Cu^2. These phenomena make it suitable for the possible detection of anions with the **BuCAC**–Cu^{2+} system.

The addition of sulfide ions (S^{2-}) to the **BuCAC**–Cu^{2+} system gradually increased the fluorescence intensity at 419 nm (Fig. 2a) because of the rapid formation of a stable product (CuS) by the sulfur ion and copper ion. With the help of this characteristic, the probe is released and the fluorescence intensity is recovered. In the concentration range of 0–14.5 μM, the change in fluorescence intensity has a good linear correlation with the concentration of S^{2-}, R^2 = 0.995 (Fig. 2b), the detection limit of **BuCAC**–Cu^{2+} for S^{2-} was found to be 1.3×10^{-7} M. Compared with other currently reported probes for Cu^{2+} and S^{2-} listed in Table S1 (ESI†).

The selectivity of probe **BuCAC**–Cu^{2+} towards S^{2-} was also investigated upon addition of various anions (F^-, Cl^-, Br^-, I^-, S^{2-}, NO_3^-, SO_3^{2-}, HSO_4^-, $H_2PO_4^-$, ClO_4^-, and CH_3COO^-) in CH_3CN : PBS (v/v = 8 : 2, pH = 7.4) solution. The results revealed that the addition of various anions into the **BuCAC**–Cu^{2+}
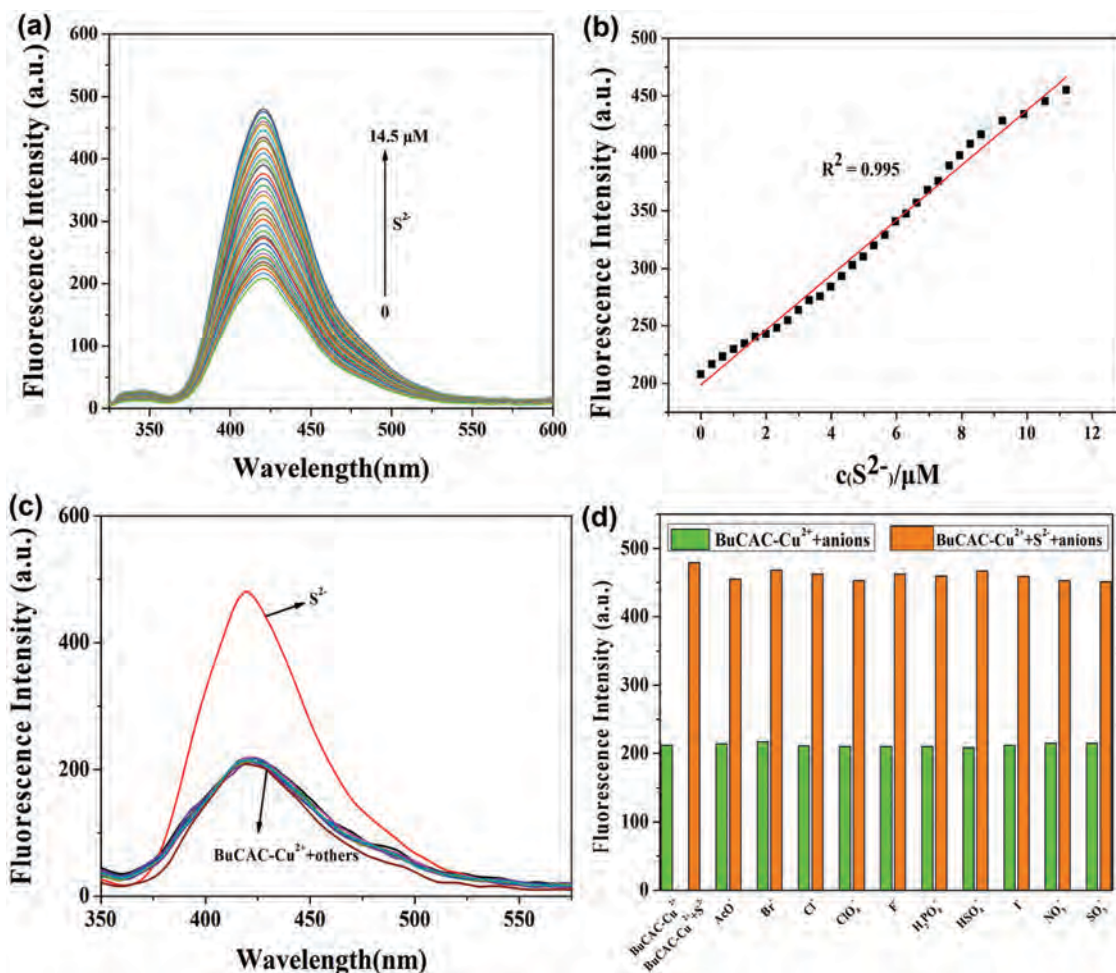
Fig. 2 (a) Fluorescence spectra of **BuCAC–Cu^{2+}** (10 μM) to S^{2-} in CH$_3$CN : PBS ((v/v = 8 : 2, pH = 7.4)) solution. (λ_{ex} = 305 nm, slit width: 5, 5 nm). (b) Linear relationship between the fluorescence intensity and concentration range of S^{2-} (0–14.5 μM). (c) Fluorescence spectra of **BuCAC–Cu^{2+}** (10 μM) in the presence of various anions (10 equiv.) in CH$_3$CN : PBS (v/v = 8 : 2, pH = 7.4), λ_{ex} = 305 nm, slit width: 5, 5 nm. (d) Fluorescence spectra of **BuCAC–Cu^{2+}** in the presence of interfering anions in CH$_3$CN : PBS ((v/v = 8 : 2, pH = 7.4)) solution.

solution did not affect the fluorescence intensity at 419 nm which was amazingly increased by S^{2-} from 210 to 480 (Fig. 2c). Moreover, the competing behavior of **BuCAC–Cu^{2+}** was studied in the presence of other anions to check the sensitivity of S^{2-}. It can be seen from Fig. 2d that the complex **BuCAC–Cu^{2+}** specifically detects the S^{2-} in the medium even in the presence of various other anions.
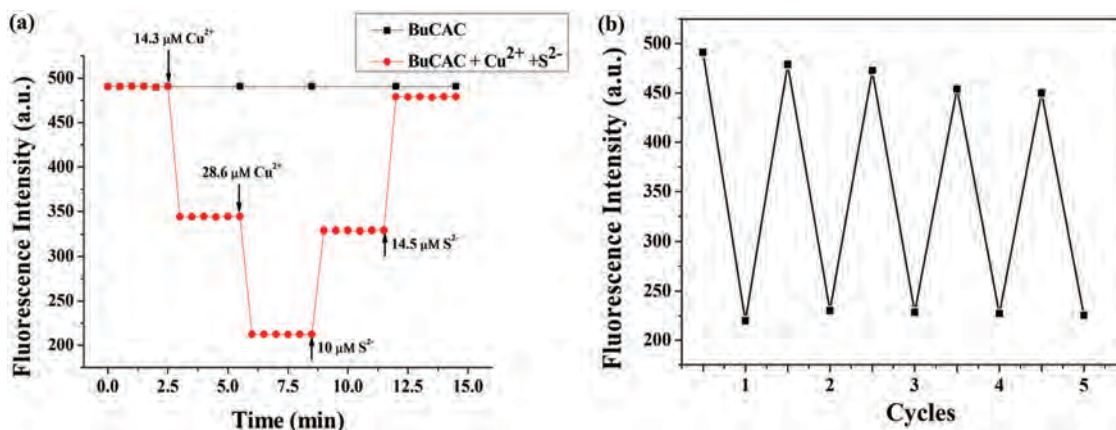

Fig. 3 (a) Time-course fluorescence responses of **BuCAC** (10 μM) towards Cu^{2+} and *in situ* produced complex **BuCAC–Cu^{2+}** to S^{2-}. (b) Fluorescence intensity of **BuCAC** (10 μM) upon the alternate addition of Cu^{2+} and S^{2-}.

3.4. The dynamics and reversibility test of BuCAC, BuCAC–Cu^{2+} and BuCAC–Cu^{2+}+ S^{2-}

Fig. 3a shows that the fluorescence intensity of the probe **BuCAC** remained unchanged with the increase of time but the intensity decreased rapidly after the addition of copper ions ($t < 30$ s).
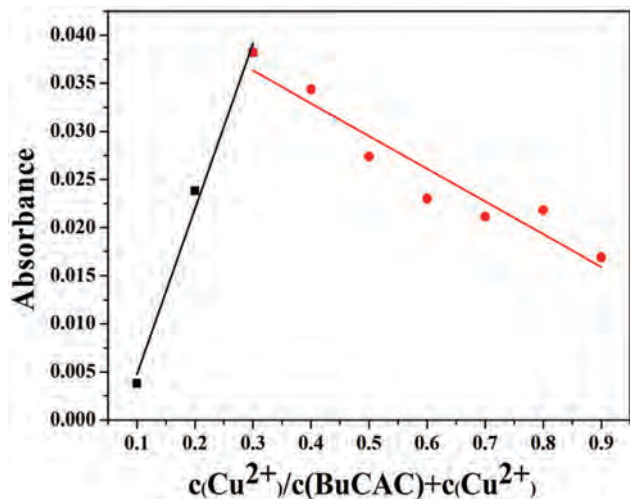
Fig. 4 Job's plot between **BuCAC** and Cu^{2+}.

However, the addition of sulfur ions caused a rapid increase in the fluorescence intensity ($t < 30$ s) and became stable.

To further study the practicability of the probe, the reversibility experiments were performed by alternate addition of Cu^{2+} and S^{2-} into **BuCAC** solution. The fluorescence intensity showed repeated quenching and recovery after adding Cu^{2+} and S^{2-}, respectively (Fig. 3b). In the meantime, the reversible inter-conversion can be repeated 5 times under low fluorescence efficiency loss, indicating that **BuCAC** has the potential to be an "on–off–on" probe for Cu^{2+} and S^{2-}.

3.5. Mechanistic research of BuCAC for sensing Cu^{2+} and BuCAC–Cu^{2+} for S^{2-}

The binding ratio of Cu^{2+} ions with **BuCAC** was investigated by using Job's plot (Fig. 4). The highest absorbance was observed with a molar fraction of 0.3, indicating the formation of **BuCAC** and Cu^{2+} as a 2 : 1 complex. According to the absorption spectra, the binding constant of **BuCAC** and Cu^{2+} was 2.4×10^4. Additionally, the experimental mass spectrum of **BuCAC**–Cu^{2+} was also studied (Fig. S5, ESI†), a mass fraction of $m/z = 711.5751$ attributed to the complex which was formed by the ligand and metal ion, $[(\text{BuCAC})_2(\text{OAc})_2\text{Cu·CH}_3\text{CN} + \text{H}]^+$, in the stoichiometric ratio of 2 : 1. The above results showed that the probe **BuCAC** can recognize copper ions through a ratio of 2 : 1 to produce a weakly
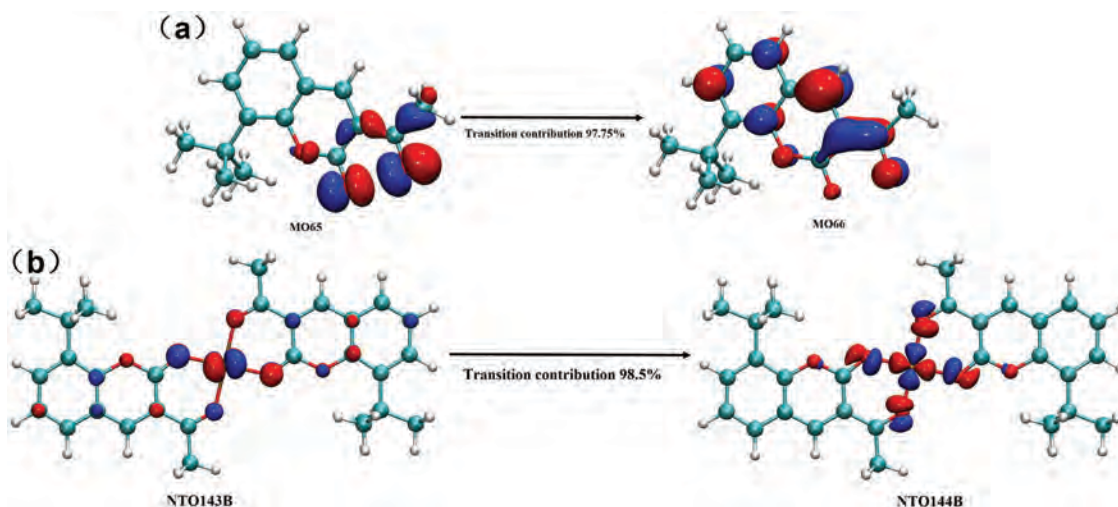

Fig. 5 (a) The orbitals involved in the principal electronic transition of **BuCAC**; (b) dominant natural transition orbital (NTO) pairs of the principal electronic transition in **BuCAC**–Cu^{2+}.
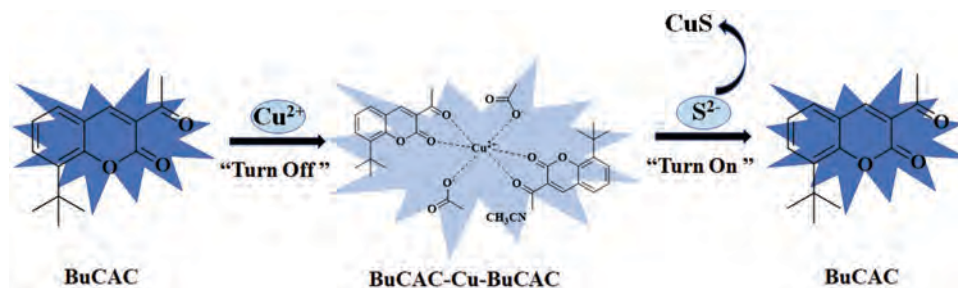

Fig. 6 The proposed sensing mechanism.

fluorescent complex **BuCAC–Cu^{2+}**. When sulfur ions were added to the system, copper ions were converted into a more stable compound copper sulfide by reacting with sulfur ions. Hence, the copper ions are removed from the complex **BuCAC–Cu^{2+}**and the original probe **BuCAC** is released with the recovery of fluorescence intensity.
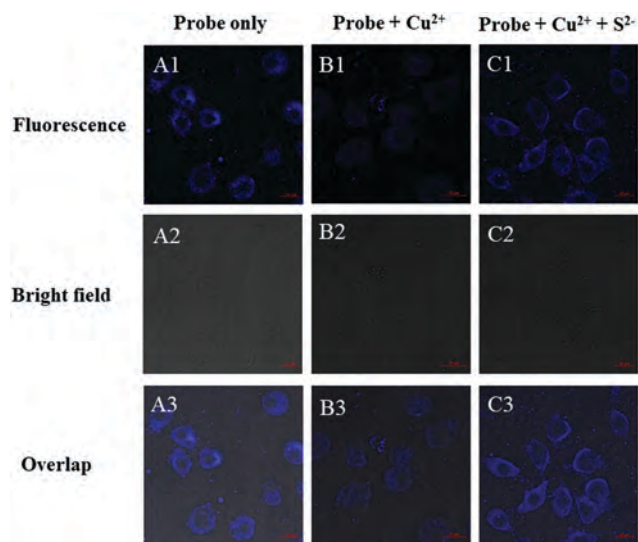

Fig. 7 CFI of HeLa cells. Cells incubated with **BuCAC** (10 μM) for 1 h (A); cells treated with Cu^{2+} (10 μM) for 60 min (B); cells treated with S^{2-} (10 μM) from **BuCAC–Cu^{2+}** for 60 min: (1) Fluorescence channel, (2) bright field, and (3) overlay image.

The sensing mechanism of **BuCAC** was also studied theoretically. Generally, the fluorescent sensors exhibit the process of charge transfer (CT). CT phenomena involved metal ions induced changes in fluorescence emission by chelation-enhanced fluorescence (CHEF) or chelation-enhanced fluorescence quenching (CHEQ) upon the chelation of a metal ion to the sensor molecule. In this sense, the CHEQ mechanism has been fully demonstrated for Cu^{2+} turn-off sensors that do not have a wavelength spectrum shift. This process is the result of the photoinduced electron transfer (PET) process.

It can be seen in Fig. 5a that the π-electrons distribute on the coumarin matrix and the acetyl skeleton on the HOMO and LUMO of **BuCAC**, the electronic transition of **BuCAC** molecule is a Local Excitation (LE), and the dominant MO transition is MO65 → MO66. The energy gaps between the HOMO and LUMO of **BuCAC** and **BuCAC–Cu^{2+}** are 4.190 eV, 3.505 eV (α orbit), and 2.796 eV (β orbit) (Table S2, ESI†). However, no dominant MO transition was observed for **BuCAC–Cu^{2+}** Hence, it is impossible to identify the nature of this excitation which was solely based on the MO pair. NTO analysis is considered an important tool to elucidate the various contributions to electron excitation. The analysis provides a compact orbital representation of electron transitions through a single configuration of hole and electron interaction. Therefore, the NTO distribution of the complex **BuCAC–Cu^{2+}** was calculated (Fig. 5b), and the optical emissions are mainly attributed to the d–d orbital transitions in the Ni atom from NTO143B to NTO144B.

Based on the results of DFT studies and mass spectrometry, the possible binding mechanism in **BuCAC–Cu^{2+}** is provided
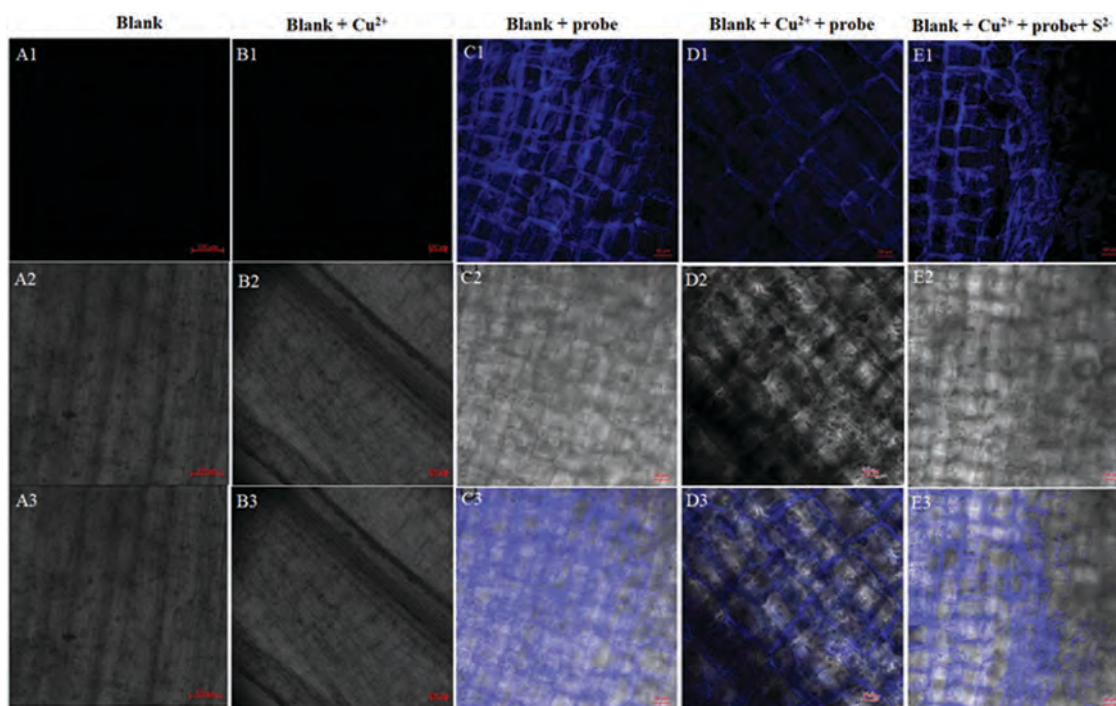

Fig. 8 CFI of soybean root tissues. CFI of soybean root tissues grown in water (A). CFI of soybean root tissues grown in the presence of Cu^{2+} (B). CFI of soybean root tissues grown in water followed by incubation with **BuCAC** (10 μM) for 1 h (C). CFI of soybean root tissues grown in the presence of Cu^{2+} followed by incubation with **BuCAC** (10 μM) for 1 h (D). CFI of soybean root tissues grown in the presence of B**uCAC–Cu^{2+}** followed by incubation with S^{2-} (10 μM) for 1 h (E): (1) Fluorescence channel, (2) bright field, and (3) overlay images.
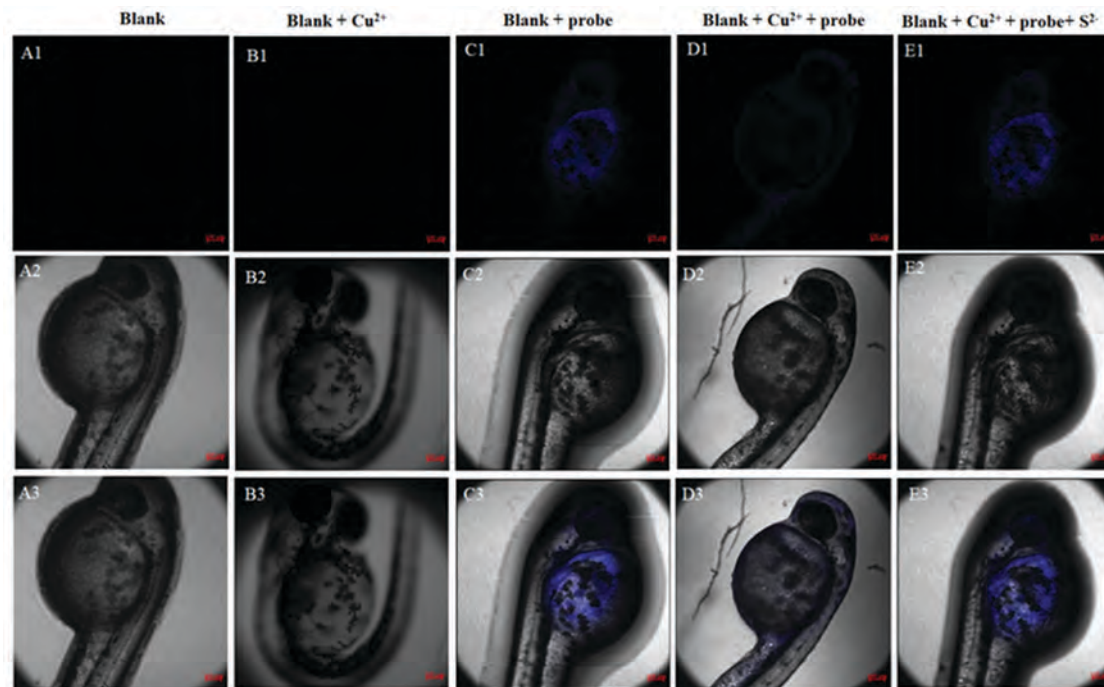
Fig. 9 CFI of zebrafish. Confocal images of zebrafish grown in water (A). CFI of zebrafish grown in a Cu^{2+}-containing environment (B). CFI of zebrafish grown in water then incubated with **BuCAC** (10 μM) for 1 h (C). CFI of zebrafish grown in a Cu^{2+}-containing environment and then incubated with **BuCAC** (10 μM) for 1 h (D). CFI of zebrafish grown in a **BuCAC–Cu^{2+}** containing environment and then incubated with **S^{2-}** (10 μM) for 1 h (E): (1) Fluorescence channel, (2) bright field, and (3) overlay images.

in Fig. 6. Cu^{2+} coordinated to the carbonyl of the acetyl group and lactone resulted in PET. The increase in energy also facilitated the existence of PET with decreased fluorescence intensity of **BuCAC–Cu^{2+}**. When S^{2-} was added to the complex **BuCAC–Cu^{2+}**, the S^{2-} combined with the Cu^{2+} and removed the Cu^{2+} from the complex, which allowed the release of the ligand and restored the fluorescence.

3.6. Cell imaging

To authenticate the potential ability of **BuCAC** in bio-imaging of Cu^{2+} and S^{2-}, the confocal fluorescence imaging application was employed for HeLa cells. Prior to conduct cell imaging experiments, the toxicity of **BuCAC** was studied and the result showed a 75% survival rate of HeLa cells, thus rendering **BuCAC** suitable for cell imaging experiments. **BuCAC** (10 μM) was injected into HeLa cells and cultivated for 1 h (Fig. 7A). Then, Cu^{2+} (10 μM) was added, which decreased the fluorescence after 60 min (Fig. 7B). While in the presence of S^{2-}, the fluorescence was restored in the fluorescence channel (Fig. 7C). The viable cells maintained their proper shape throughout the imaging experiments as evidenced by bright-field photographs and overlays of confocal fluorescence images (CFI). The obtained results suggested that probe **BuCAC** can cross the cell membrane, and hence, it can be safely applied in biological cells for fluorescence imaging of Cu^{2+} and S^{2-}.

3.7. Biological imaging

Biological imaging was carried out in soybean root tissue and zebrafish because of their enhanced water content and excellent transparency. After ethanol-based sterilization, soybean seeds were then cultured at room temperature in a moist environment. Soya was grown in a Cu^{2+}-containing environment with a fluorescence response (Fig. 8A–C). Fortunately, the fluorescence intensity turned weak upon the addition of **BuCAC** for 1 h (Fig. 8D). Besides, after the addition of S^{2-}, the fluorescence intensity recovered (Fig. 8E). The same phenomenon was also seen in zebrafish (Fig. 9). The results of the study indicated that **BuCAC** is highly biocompatible and offers a good perspective for the detection of S^{2-} and Cu^{2+} in the living body.

4. Conclusion

We successfully demonstrated the condensed product of coumarin, **BuCAC**, as a fluorescent probe for the detection of Cu^{2+} and S^{2-}. According to the fluorescence spectrum, specific fluorescence quenching was observed in the presence of Cu^{2+} within a detection limit of 3.03×10^{-7} M. **BuCAC** formed a complex in a ratio of 2 : 1 with Cu^{2+} with a binding constant of 2.4×10^4. Furthermore, **BuCAC–Cu^{2+}** can also be used to detect S^{2-} with a detection limit of 1.7×10^{-7} M. The *in vivo* detection of Cu^{2+} and S^{2-} was also studied successfully by using HeLa cells, zebrafish, and soybean root tissues.

Author contributions

Lu Sun, Lingcen Shao, Mengmeng Huang, and Hongyu Ren: synthesis and testing of probe properties. Jichao Chen, Yanqin Wang, and

Shilong Yang: software, validation. Li Xu: supervision. Jiuzhou Shi: bioimaging of HeLa cells, zebrafish, and soybean root tissue. Wen Lu: conceptualization, writing- reviewing and editing.

Conflicts of interest

The authors declare that they have no known competing financial interests or personal relationships that could have appeared to influence the work reported in this paper.

Acknowledgements

Notes and references

1 J. Wang, J. Liang, X. Liu, H. Xiao, F. P. Dong, Y. L. Wang, X. Shu, F. R. Huang and H. B. Liu, *Spectrochim. Acta, Part A*, 2019, **215**, 260–265.

2 L. S. Cui, J. U. Kim, H. Nomura, H. Nakanotani and C. Adachi, *Angew. Chem., Int. Ed.*, 2016, **128**, 6864–6868.

3 K. S. Mani, R. Rajamanikandan, B. Murugesapandian, R. Shankar, G. Sivaraman, M. Ilanchelian and S. P. Rajendra, *Spectrochim. Acta, Part A*, 2019, **214**, 170–176.

4 E. L. Que, D. W. Domaille and C. J. Chang, *Chem. Rev.*, 2018, **108**, 1517–1549.

5 K. J. Barnham and A. I. Bush, *Chem. Soc. Rev.*, 2014, **43**, 6727–6749.

6 Y. F. Tan, N. O' Toole and N. L. A. H. Taylor, *Plant Physiol.*, 2010, **152**, 747–761.

7 H. Shoaee, M. Roshdi, N. Khanlarzadeh and A. Beiraghi, *Spectrochim. Acta, Part A*, 2012, **98**, 70–75.

8 P. Zatta and A. Frank, *Brain Res. Rev.*, 2007, **54**, 19–33.

9 A. Gupte and R. J. Mumper, *Cancer Treat. Rev.*, 2009, **35**, 32–46.

10 G. Meloni, P. Faller and M. Vasak, *J. Biol. Chem.*, 2007, **282**, 16068–16078.

11 E. J. Margalioth, J. G. Schenker and M. Chevion, *Cancer*, 2015, **52**, 868–872.

12 X. L. Zuo, J. M. Chen, X. Zhou, X. Z. Li and G. Y. Mei, *Biol. Trace Elem. Res.*, 2006, **114**, 41–53.

13 U. Carpentieri, J. Myers, L. Thorpe, C. W. Daeschner and M. E. Haggard, *Cancer Res.*, 1986, **46**, 981–984.

14 K. W. Kuo, S. F. Chen, C. C. Wu, D. R. Chen and J. H. Lee, *Biol. Trace Elem. Res.*, 2002, **89**, 1–11.

15 A. Scanni, L. Licciardello, M. Trovato, M. Tomirotii and M. Biraghi, *Tumori*, 1977, **63**, 175–180.

16 A. Chan, F. Wong and M. Arumanayagam, *Ann. Clin. Biochem.*, 1993, **30**, 545–549.

17 Q. Z. Dai, C. M. Gao, Y. J. Liu, H. Y. Liu, B. R. Xiao, C. K. Chen, J. W. Chen, Z. G. Yuan and Y. Y. Jiang, *Tetrahedron*, 2018, **74**, 6459–6464.

18 A. Farhi, F. Firdaus, H. Saeed, A. Mujeeb, M. Shakira and M. Owaisc, *Photochem. Photobiol. Sci.*, 2019, **18**, 3008–3015.

19 F. Abebe, P. Perkins, R. Shaw and S. Tadesse, *J. Mol. Struct.*, 2020, **1205**, 127594.

20 H. Hosseinjani-Pirdehi, N. O. A. Mahmoodi, A. Taheri, K. A. A. Asalemi and R. Esmaeili, *Spectrochim. Acta, Part A*, 2020, **229**, 117989.

21 F. Y. Yan, X. D. Sun, R. Q. Zhang, Y. X. Jiang, J. X. Xu and J. F. Wei, *Spectrochim. Acta, Part A*, 2019, **222**, 117222.

22 C. Long, J. H. Hu, Q. Q. Fu and P. W. Ni, *Spectrochim. Acta, Part A*, 2019, **219**, 297–306.

23 Y. K. Xu, L. Yang, H. Y. Wang, Y. X. Zhang, X. F. Yang, M. S. Pei and G. Y. Zhang, *J. Photochem. Photobiol., A*, 2020, **391**, 112372.

24 X. C. Li, Y. J. Han, S. S. Sun, D. D. Shan, X. M. Ma, G. J. He, N. Mergu, J. S. Park, C. H. Kim and Y. A. Son, *Spectrochim. Acta, Part A*, 2020, **233**, 118179.

25 H. Chen, P. Yang, Y. H. Li, L. L. Zhang, F. Ding, X. J. He and J. L. Shen, *Spectrochim. Acta, Part A*, 2020, **224**, 117384.

26 C. B. Bai, H. Y. Fan, R. Qiao, S. N. Wang, B. Wei, Q. Meng, Z. Q. Wang, J. X. Liao, J. Zhang, L. Zhang, S. S. Chen and H. Miao, *Spectrochim. Acta, Part A*, 2016, **216**, 45–51.

27 Y. Xie, L. Q. Yan and J. P. Li, *Appl. Spectrosc.*, 2019, **73**, 794–800.

28 X. Wang, T. Qin, S. S. Bao, Y. C. Zhang, X. Shen, L. M. Zheng and D. R. Zhu, *J. Mater. Chem. A*, 2016, **4**, 16484–16489.

29 J. Qu, Q. X. Xia, W. Ji, S. Jing, D. R. Zhu, L. Lin, L. Huang, Z. F. An, C. Q. Xin, Y. Ni, M. X. Li, J. D. Jia, Y. L. Song and W. Huang, *Dalton Trans.*, 2018, **47**, 1479–1487.

30 R. Huang, X. Zheng and Y. Qu, *Anal. Chim. Acta*, 2007, **582**, 267–274.

31 K. Eto, T. Asada, K. Arima and H. Kimura, *Biophys. Res. Commun.*, 2002, **293**, 1485–1488.

32 P. Kamoun, M. C. Belardinelli, A. Chabli and K. Lallouchi, *Am. J. Med. Genet., Part A*, 2020, **116A**, 310–311.

33 W. Yang, G. D. Yang, X. M. Jia and L. Y. Wu, *J. Physiol.*, 2005, **569**, 519–531.

34 S. Fiorucci, E. Antonelli, A. Mencarelli and S. Orlandi, *Hepatology*, 2005, **42**, 539–548.

35 T. D. Ashton, K. A. Jolliffe and F. M. Pfeffer, *Chem. Soc. Rev.*, 2015, **44**, 4547–4595.

36 W. Xu, L. Zhu, X. Shao, K. Huang and Y. Luo, *Biosens. Bioelectron.*, 2018, **120**, 168–174.

37 R. K. Singh, B. Panigrahi, S. Mishra, B. Das, R. Jayabalan, P. K. Parhi and D. Mandal, *J. Mol. Liq.*, 2018, **269**, 269–277.

38 T. Liu, Y. Luo, L. Kong, J. Zhu, W. Wang and L. Tan, *Sens. Actuators, B*, 2016, **235**, 568–574.

39 J. E. Doeller, T. S. Isbell, G. Benavides, J. Koenitzer, H. Patel, R. P. Patel, J. R. Lancaster, V. M. Darley-Usmar and D. W. Kraus, *Anal. Biochem.*, 2005, **341**, 40–51.

40 J. R. Knaery and G. A. Cutter, *Anal. Chem.*, 1993, **65**, 976–982.

41 Y. Shen, X. Zhang, C. Zhang, Y. Zhang, J. Jin and H. Li, *Spectrochim. Acta, Part A*, 2018, **191**, 427–434.

42 C. Li, Z. Liu, Y. Miao, X. Zhou and X. Wu, *Dyes Pigm.*, 2016, **125**, 292–298.

43 J. C. Qin and Z. Y. Yang, *Mater. Sci. Eng., C*, 2015, **57**, 265–271.

44 Y. Q. Hao, W. S. Chen, L. Q. Wang, X. Zhu, Y. T. Zhang, P. Qu, L. Liu, B. B. Zhou, Y. N. Liu and M. T. Xu, *Talanta*, 2015, **143**, 307–314.

45 A. K. Mahapatra, S. Mondal, S. K. Manna, K. Maiti and R. Maji, *Dalton Trans.*, 2015, **44**, 6490–6501.

46 L. J. Hou, J. B. Chao, Y. Wang, Y. S. Wang, S. M. Shuang, C. Z. Li, X. Y. Kong and C. Dong, *J. Mater. Chem. B*, 2017, **5**, 8957–8966.

47 M. J. Frisch, G. W. Trucks, H. B. Schlegel, G. E. Scuseria, M. A. Robb, J. R. Cheeseman, G. Scalmani, V. Barone, G. A. Petersson, H. Nakatsuji, X. Li, M. Caricato, A. V. Marenich, J. Bloino, B. G. Janesko, R. Gomperts, B. Mennucci, H. P. Hratchian, J. V. Ortiz, A. F. Izmaylov, J. L. Sonnenberg, D. Williams-Young, F. Ding, F. Lipparini, F. Egidi, J. Goings, B. Peng, A. Petrone, T. Henderson, D. Ranasinghe, V. G. Zakrzewski, J. Gao, N. Rega, G. Zheng, W. Liang, M. Hada, M. Ehara, K. Toyota, R. Fukuda, J. Hasegawa, M. Ishida, T. Nakajima, Y. Honda, O. Kitao, H. Nakai, T. Vreven, K. Throssell, J. A. Montgomery, Jr., J. E. Peralta, F. Ogliaro, M. J. Bearpark, J. J. Heyd, E. N. Brothers, K. N. Kudin, V. N. Staroverov, T. A. Keith, R. Kobayashi, J. Normand, K. Raghavachari, A. P. Rendell, J. C. Burant, S. S. Iyengar, J. Tomasi, M. Cossi, J. M. Millam, M. Klene, C. Adamo, R. Cammi, J. W. Ochterski, R. L. Martin, K. Morokuma, O. Farkas, J. B. Foresman and D. J. Fox, *Gaussian 16, Revision C.01*, Gaussian, Inc., Wallingford CT, 2019.

48 A. D. Becke, *J. Chem. Phys.*, 1993, **98**, 5648–5652.

49 R. Krishnan, J. S. Binkley, R. Seeger and J. A. Pople, *J. Chem. Phys.*, 1980, **72**, 650–654.

50 K. Raghavachari and G. W. Trucks, *J. Chem. Phys.*, 1989, **91**, 1062–1065.

51 S. Grimme, J. Antony, S. Ehrlich and H. Krieg, *J. Chem. Phys.*, 2010, **132**, 154104.

52 R. L. Martin, *J. Chem. Phys.*, 2003, **118**, 4775–4777.

53 A. V. Marenich, C. Cramer and D. G. Truhlar, *J. Phys. Chem. B*, 2009, **113**, 6378–6396.